

DISCRETE-ORDINATE DISCONTINUOUS GALERKIN METHODS FOR SOLVING THE RADIATIVE TRANSFER EQUATION*

WEIMIN HAN[†], JIANGUO HUANG[‡], AND JOSEPH A. EICHHOLZ[§]

Abstract. The radiative transfer equation (RTE) occurs in a wide variety of applications. In this paper, we study discrete-ordinate discontinuous Galerkin methods for solving the RTE. The numerical methods are formed in two steps. In the first step, the discrete ordinate technique is applied to discretize the integral operator for the angular variable, resulting in a semidiscrete hyperbolic system. In the second step, the spatial discontinuous Galerkin method is applied to discretize the semidiscrete system. A stability and error analysis is performed on the numerical methods. Some numerical examples are included to demonstrate the convergence behavior of the methods.

Key words. radiative transfer equation, discrete-ordinate discontinuous Galerkin method, stability, convergence, error estimation

AMS subject classifications. 65N30, 65R20

DOI. 10.1137/090767340

1. Introduction. Radiative transfer theory describes the interaction of radiation with scattering and absorbing media, which has wide applications in such areas as neutron transport, heat transfer, stellar atmospheres optical molecular imaging, infrared and visible light in space and the atmosphere, and so on. We refer to [2, 7, 19, 27, 28, 31, 32] and references therein for details about this subject. In the stationary one-velocity case, the photon (neutron) intensity, a function of three space variables \mathbf{x} and two angular variables ω , is governed mathematically by the radiative transfer equation (RTE) (cf. [2, 25])

$$\omega \cdot \nabla u(\mathbf{x}, \omega) + \sigma_t(\mathbf{x}) u(\mathbf{x}, \omega) = \sigma_s(\mathbf{x}) \int_{\Omega} g(\mathbf{x}, \omega \cdot \hat{\omega}) u(\mathbf{x}, \hat{\omega}) d\sigma(\hat{\omega}) + f(\mathbf{x}, \omega).$$

Here σ_t , σ_s , g , and f are given functions, and Ω denotes the unit sphere in \mathbb{R}^3 . The RTE can be viewed as a hyperbolic-type integro-differential equation. Due to this complication and the high dimension of the problem, it is a serious challenge to develop effective numerical methods for RTE, a topic that attracted much attention in the past five decades. The numerical methods used today include discrete ordinate methods, methods using spherical harmonics, finite difference methods, finite element methods and spectral methods, and so on. We refer to [25] for a basic and comprehensive understanding about this context. Among all the methods just mentioned, the discrete ordinate method (cf. [11, 25]) has received significant attention and devel-

*Received by the editors August 6, 2009; accepted for publication (in revised form) November 2, 2009; published electronically February 17, 2010.

<http://www.siam.org/journals/sisc/32-2/76734.html>

[†]Department of Mathematics, University of Iowa, Iowa City, IA 52242 (whan@math.uiowa.edu). The work of this author was partially supported by the Mathematical and Physical Sciences Funding Program of University of Iowa.

[‡]Department of Mathematics, Shanghai Jiao Tong University, Shanghai 200240, China; Division of Computational Science, E-Institute of Shanghai Universities, Shanghai Normal University, China; Scientific Computing Key Laboratory of Shanghai Universities, China (jghuang@sjtu.edu.cn). The work of this author was partially supported by the National Basic Research Program (2005CB321701), NNSFC (10371076), and E-Institutes of Shanghai Municipal Education Commission (E03004).

[§]Department of Mathematics, University of Iowa, Iowa City, IA 52242 (jeichhol@math.uiowa.edu).

opment, owing to the good compromise between accuracy, flexibility, and moderate computational requirements. A number of discrete ordinate methods combined with Chebyshev spectral methods were introduced in [4, 17, 23] for solving RTE in regular space domains; in [12], a spatial multigrid algorithm was presented for isotropic neutron transport in x - y geometry, where the linear system to be solved is obtained using discrete ordinates in angle and corner balance finite differencing in space.

Since RTE is essentially a hyperbolic-type system, it is natural to solve the problem by the discrete ordinate method combined with the discontinuous Galerkin (DG) discretization in space. We call the resulting methods discrete-ordinate DG methods. Here we briefly review some advances of DG methods related to our problem under consideration. In 1973, Reed and Hill introduced in [29] the first DG method for linear hyperbolic problems (the neutron transport equation without scattering term), and the error analysis of the method was established thoroughly in [22, 24]. A comprehensive introduction of DG methods was given in [15], for computational fluid dynamics. A general framework was presented in [14] for constructing DG methods based on the discrete stability identities, from which one can derive many efficient DG methods for a large number of partial differential equations (systems) in a unified way. The stabilization mechanism frequently used in DG methods was revealed in [9], and the theory is also applied to discuss DG methods for linear hyperbolic problems. In addition, a complete study about the latter problem was given in [10], and some optimal error estimates in certain discrete norm were obtained there too. In [26], a DG method was proposed for solving the one-dimensional spherical neutron transport equation without scattering term. DG methods have also been applied successfully to solve elliptic problems (cf. [3]) and many other mathematical physical problems (cf. [16]).

To derive our discrete-ordinate DG methods, we first replace the scattering term (integral term) in RTE by a certain quadrature sum and require only that the resulting equations are valid at all angular directions corresponding to the numerical integration nodes, resulting in a linear first-order hyperbolic system. Then, following [9, 10, 15], we further discretize this system by DG methods to get some fully discrete methods for solving RTE in any geometric shape domains in space. As in [9, 10], we also consider the DG methods for which a certain stabilization term is added for penalizing the jump of the solution across interior faces of the triangulation, in order to get numerical solutions with physical sense in practical applications. For error analysis of our methods, we first give a simple abstract lemma for error estimates of general DG methods, which is similar to the second Strang lemma in error analysis of nonconforming element methods (cf. [13]). Then, we establish some stability estimates for our methods in certain discrete norm, which, in conjunction with the previous lemma and some careful estimates involving a certain L^2 -orthogonal projection operator, leads to some error estimates between the semidiscrete solution and the numerical solutions. Using an error formula for the numerical quadrature on the unit sphere (cf. [21]) and the energy integration method, we obtain an error bound between the exact solution and the semidiscrete solution in the L^2 -norm. These estimates together give rise to error estimates between the exact solution and our numerical solutions in the L^2 -norm. Numerical results from several examples are provided to illustrate computational performance of the methods proposed here.

We end this section by introducing some notation frequently used later on. Throughout this paper, we will use the standard notation for Sobolev spaces together with their norms and seminorms (cf. [1, 6, 8]). For instance, for an open set D in \mathbb{R}^3 , $H^1(D)$ is the space of all square-integrable functions whose first-order weak derivatives are also square-integrable in D ; for any $v \in H^1(D)$, its norm and seminorm in

$H^1(D)$ are defined by

$$\|v\|_{1,D} = \left[\int_D (|v|^2 + |\nabla v|^2) dx \right]^{1/2}, \quad |v|_{1,D} = \left(\int_D |\nabla v|^2 dx \right)^{1/2},$$

where ∇ stands for the gradient operator with respect to the \mathbf{x} variable. Moreover, for any two real quantities a and b , the symbol $a \lesssim b$ abbreviates $a \leq Cb$, with C a positive constant independent of the finite element mesh size, which may take different values at different appearances.

2. The radiative transfer equation. Let X be a domain in \mathbb{R}^3 with a Lipschitz boundary ∂X . Note that the unit outward normal $\mathbf{n}(\mathbf{x})$ exists a.e. on ∂X . Denote by Ω the unit sphere in \mathbb{R}^3 . For each fixed direction $\boldsymbol{\omega} \in \Omega$, introduce a new Cartesian coordinate system (z_1, z_2, s) by the relations

$$\mathbf{x} = \mathbf{z} + s\boldsymbol{\omega}, \quad \mathbf{z} = z_1\boldsymbol{\omega}_1 + z_2\boldsymbol{\omega}_2,$$

where $(\boldsymbol{\omega}, \boldsymbol{\omega}_1, \boldsymbol{\omega}_2)$ is an orthonormal basis of \mathbb{R}^3 , $z_1, z_2, s \in \mathbb{R}$. With respect to this new coordinate system, we denote by $X_\boldsymbol{\omega}$ the projection of X on the plane $s = 0$ in \mathbb{R}^3 and by $X_{\boldsymbol{\omega}, \mathbf{z}}$ ($\mathbf{z} \in X_\boldsymbol{\omega}$) the intersection of the straight line $\{\mathbf{z} + s\boldsymbol{\omega}; s \in \mathbb{R}\}$ with X . We assume that the domain X is such that for any $(\boldsymbol{\omega}, \mathbf{z})$ with $\mathbf{z} \in X_\boldsymbol{\omega}$, $X_{\boldsymbol{\omega}, \mathbf{z}}$ is the union of a finite number of line segments:

$$X_{\boldsymbol{\omega}, \mathbf{z}} = \bigcup_{i=1}^{N(\boldsymbol{\omega}, \mathbf{z})} \{\mathbf{z} + s\boldsymbol{\omega}; s \in (s_{i,-}, s_{i,+})\}.$$

Here $s_{i,\pm} = s_{i,\pm}(\boldsymbol{\omega}, \mathbf{z})$ depend on $\boldsymbol{\omega}$ and \mathbf{z} , and $\mathbf{x}_{i,\pm} := \mathbf{z} + s_{i,\pm}\boldsymbol{\omega}$ are the intersection points of the line $\{\mathbf{z} + s\boldsymbol{\omega}; s \in \mathbb{R}\}$ with ∂X . We further assume $\sup_{\boldsymbol{\omega}, \mathbf{z}} N(\boldsymbol{\omega}, \mathbf{z}) < \infty$, known as a generalized convexity condition. As an example, for a convex domain X , $\sup_{\boldsymbol{\omega}, \mathbf{z}} N(\boldsymbol{\omega}, \mathbf{z}) = 1$. We then introduce the following subsets of ∂X :

$$\begin{aligned} \partial X_{\boldsymbol{\omega}, -} &= \{\mathbf{z} + s_{i,-}\boldsymbol{\omega}; 1 \leq i \leq N(\boldsymbol{\omega}, \mathbf{z}), \mathbf{z} \in X_\boldsymbol{\omega}\}, \\ \partial X_{\boldsymbol{\omega}, +} &= \{\mathbf{z} + s_{i,+}\boldsymbol{\omega}; 1 \leq i \leq N(\boldsymbol{\omega}, \mathbf{z}), \mathbf{z} \in X_\boldsymbol{\omega}\}. \end{aligned}$$

It can be shown that if $\mathbf{n}(\mathbf{x}_{i,-})$ exists with $\mathbf{x}_{i,-} = \mathbf{z} + s_{i,-}\boldsymbol{\omega}$, then $\mathbf{n}(\mathbf{x}_{i,-}) \cdot \boldsymbol{\omega} \leq 0$; if $\mathbf{x} \in \partial X$ and $\mathbf{n}(\mathbf{x}) \cdot \boldsymbol{\omega} < 0$, then $\mathbf{x} \in \partial X_{\boldsymbol{\omega}, -}$. Likewise, if $\mathbf{n}(\mathbf{x}_{i,+})$ exists with $\mathbf{x}_{i,+} = \mathbf{z} + s_{i,+}\boldsymbol{\omega}$, then $\mathbf{n}(\mathbf{x}_{i,+}) \cdot \boldsymbol{\omega} \geq 0$; if $\mathbf{x} \in \partial X$ and $\mathbf{n}(\mathbf{x}) \cdot \boldsymbol{\omega} > 0$, then $\mathbf{x} \in \partial X_{\boldsymbol{\omega}, +}$. Now, define

$$\Gamma_- = \{(\mathbf{x}, \boldsymbol{\omega}); \mathbf{x} \in \partial X_{\boldsymbol{\omega}, -}, \boldsymbol{\omega} \in \Omega\}, \quad \Gamma_+ = \{(\mathbf{x}, \boldsymbol{\omega}); \mathbf{x} \in \partial X_{\boldsymbol{\omega}, +}, \boldsymbol{\omega} \in \Omega\}$$

for the incoming and outgoing boundaries. Both are subsets of $\Gamma = \partial X \times \Omega$.

Denote by $d\sigma(\boldsymbol{\omega})$ the infinitesimal area element on the unit sphere Ω . If we introduce the spherical coordinate system by

$$(2.1) \quad \boldsymbol{\omega} = (\sin \theta \cos \psi, \sin \theta \sin \psi, \cos \theta)^T, \quad 0 \leq \theta \leq \pi, 0 \leq \psi \leq 2\pi,$$

then $d\sigma(\boldsymbol{\omega}) = \sin \theta d\theta d\psi$. We will need an integral operator S defined by

$$(2.2) \quad (Su)(\mathbf{x}, \boldsymbol{\omega}) = \int_{\Omega} g(\mathbf{x}, \boldsymbol{\omega} \cdot \hat{\boldsymbol{\omega}}) u(\mathbf{x}, \hat{\boldsymbol{\omega}}) d\sigma(\hat{\boldsymbol{\omega}}),$$

with g a nonnegative normalized phase function

$$(2.3) \quad \int_{\Omega} g(\mathbf{x}, \boldsymbol{\omega} \cdot \hat{\boldsymbol{\omega}}) d\sigma(\hat{\boldsymbol{\omega}}) = 1 \quad \forall \mathbf{x} \in X, \boldsymbol{\omega} \in \Omega.$$

In most applications, the function g is independent of \mathbf{x} . One well-known example is the Henyey–Greenstein phase function (cf. [20])

$$(2.4) \quad g(t) = \frac{1 - \eta^2}{4\pi(1 + \eta^2 - 2\eta t)^{3/2}}, \quad t \in [-1, 1],$$

where the parameter $\eta \in (-1, 1)$ is the anisotropy factor of the scattering medium. Note that $\eta = 0$ for isotropic scattering, $\eta > 0$ for forward scattering, and $\eta < 0$ for backward scattering.

With the above notation, a boundary value problem of the RTE reads (cf. [2,25])

$$(2.5) \quad \boldsymbol{\omega} \cdot \nabla u(\mathbf{x}, \boldsymbol{\omega}) + \sigma_t(\mathbf{x}) u(\mathbf{x}, \boldsymbol{\omega}) = \sigma_s(\mathbf{x}) (Su)(\mathbf{x}, \boldsymbol{\omega}) + f(\mathbf{x}, \boldsymbol{\omega}), \quad (\mathbf{x}, \boldsymbol{\omega}) \in X \times \Omega,$$

$$(2.6) \quad u(\mathbf{x}, \boldsymbol{\omega}) = 0, \quad (\mathbf{x}, \boldsymbol{\omega}) \in \Gamma_-.$$

Here $\sigma_t = \sigma_a + \sigma_s$, σ_a is the macroscopic absorption cross section, σ_s is the macroscopic scattering cross section, and f is a source function. We assume these given functions satisfy

$$(2.7) \quad \sigma_t, \sigma_s \in L^\infty(X), \quad \sigma_s \geq 0 \text{ a.e. in } X, \quad \sigma_t - \sigma_s \geq c_0 \text{ in } X \text{ for a const. } c_0 > 0,$$

$$(2.8) \quad f(\mathbf{x}, \boldsymbol{\omega}) \in L^2(X \times \Omega) \text{ and is a continuous function with respect to } \boldsymbol{\omega} \in \Omega.$$

These assumptions are naturally valid in applications; the last part of (2.7) means that the absorption effect is not negligible. The homogeneous boundary condition (2.6) corresponds to a vacuum setting around X . It is equally well to consider a general incoming flux boundary condition $u(\mathbf{x}, \boldsymbol{\omega}) = u_{\text{in}}(\mathbf{x}, \boldsymbol{\omega})$ on Γ_- with a given function u_{in} .

It is shown in [2] that the problem (2.5)–(2.6) has a unique solution $u \in H_2^1(X \times \Omega)$, where

$$H_2^1(X \times \Omega) := \{v \in L^2(X \times \Omega); \boldsymbol{\omega} \cdot \nabla v \in L^2(X \times \Omega)\}$$

with $\boldsymbol{\omega} \cdot \nabla v$ denoting the generalized directional derivative of v in the direction $\boldsymbol{\omega}$ (cf. [2]).

3. Discrete-ordinate DG methods. In order to define our discrete-ordinate DG methods for the problem (2.5)–(2.6), we first approximate the integration term Su appearing in (2.5) by certain quadrature. We write the numerical quadrature to be used in the form

$$(3.1) \quad \int_{\Omega} F(\boldsymbol{\omega}) d\sigma(\boldsymbol{\omega}) \approx \sum_{l=1}^L w_l F(\boldsymbol{\omega}_l), \quad w_l > 0, \quad \boldsymbol{\omega}_l \in \Omega, \quad 1 \leq l \leq L,$$

where F is a continuous function over the unit sphere Ω . One family of quadratures is given by the product numerical integration formulas (cf. [5,30]), e.g., for a positive integer m , with $L = 2m^2$,

$$(3.2) \quad \int_{\Omega} F(\boldsymbol{\omega}) d\sigma(\boldsymbol{\omega}) = \int_0^{2\pi} \int_0^{\pi} \bar{F}(\theta, \psi) \sin \theta d\theta d\psi \approx \frac{\pi}{m} \sum_{j=1}^{2m} \sum_{i=1}^m w_i \bar{F}(\theta_i, \psi_j)$$

in the spherical coordinate system (2.1). Here \bar{F} stands for the representation of F in the spherical coordinates, and $\{\theta_i\}$ are chosen so that $\{\cos \theta_i\}$ and $\{w_i\}$ are the

Gauss–Legendre nodes and weights on $[-1, 1]$. The points $\{\psi_j\}$ are evenly spaced on $[0, 2\pi]$ with a spacing π/m ; typically,

$$\psi_j = j\pi/m \text{ or } (j - 1/2)\pi/m.$$

With the above choice of node points and weights, the numerical quadrature (3.2) integrates exactly any polynomial $F(\mathbf{x})$ of a total degree no more than $2m - 1$. A popular choice of quadratures in relevant engineering literature is the $\{S_N\}$ family that has prescribed geometric symmetry for the set of the quadrature nodes on the unit sphere, and we refer to [11, 25] for details along this line. Our error analysis of the discrete-ordinate DG methods work for general quadratures of the form given in (3.1). Then the integral operator S can be approximated by a discretized operator S_d given by

$$(3.3) \quad S_d u(\mathbf{x}, \boldsymbol{\omega}) = \sum_{l=1}^L w_l g(\mathbf{x}, \boldsymbol{\omega} \cdot \boldsymbol{\omega}_l) u(\mathbf{x}, \boldsymbol{\omega}_l).$$

Regarding the accuracy of the quadrature (3.1), we will write n for the degree of precision of the quadrature, i.e., the quadrature integrates exactly all spherical polynomials (cf. [18]) of total degree no more than n and does not integrate exactly some spherical polynomial of total degree $n + 1$. Then by [21, Corollary 6],

$$(3.4) \quad \left| \int_{\Omega} F(\boldsymbol{\omega}) d\sigma(\boldsymbol{\omega}) - \sum_{l=1}^L w_l F(\boldsymbol{\omega}_l) \right| \leq c_s n^{-s} \|F\|_{s,\Omega} \quad \forall F \in H^s(\Omega), s > 1.$$

Here $H^s(\Omega)$ is the Sobolev space of order s over Ω (cf. [18]), and c_s is a universal constant depending only on s .

Associated with the numerical quadrature (3.1), define

$$(3.5) \quad m(\mathbf{x}) = \max_{1 \leq i \leq L} \sum_{l=1}^L w_l g(\mathbf{x}, \boldsymbol{\omega}_l \cdot \boldsymbol{\omega}_i)$$

and make the following assumption:

$$(3.6) \quad \sigma_t - m \sigma_s \geq c'_0 \text{ in } X \text{ for some constant } c'_0 > 0.$$

This assumption will be needed in our error analysis in section 4. Note that the summation $\sum_{l=1}^L w_l g(\mathbf{x}, \boldsymbol{\omega}_l \cdot \boldsymbol{\omega}_i)$ is an approximation of the integral $\int_{\Omega} g(\mathbf{x}, \boldsymbol{\omega}_i \cdot \boldsymbol{\omega}) d\sigma(\boldsymbol{\omega})$, which equals 1 by the normalization condition (2.3). If $g(\mathbf{x}, \hat{\boldsymbol{\omega}} \cdot)$ is an $H^s(\Omega)$ ($s > 1$) function for any fixed $\mathbf{x} \in X$ and $\hat{\boldsymbol{\omega}} \in \Omega$, then by (3.4),

$$\left| 1 - \sum_{l=1}^L w_l g(\mathbf{x}, \boldsymbol{\omega}_i \cdot \boldsymbol{\omega}_l) \right| \leq c_s n^{-s} \|g(\mathbf{x}, \boldsymbol{\omega}_i \cdot)\|_{s,\Omega}.$$

Thus, $m(\mathbf{x})$ is close to 1 if the numerical quadrature has certain degree of precision, at least when the function $\boldsymbol{\omega} \mapsto g(\mathbf{x}, \hat{\boldsymbol{\omega}} \cdot \boldsymbol{\omega})$ is in $H^s(\Omega)$ with some $s > 1$, for any $\mathbf{x} \in X$ and $\hat{\boldsymbol{\omega}} \in \Omega$. Hence, under the assumption (2.7), (3.6) is not a very restrictive condition. For the Henyey–Greenstein phase function (2.4), we actually have

$$\left| 1 - \sum_{l=1}^L w_l g(\boldsymbol{\omega}_i \cdot \boldsymbol{\omega}_l) \right| \leq c_s n^{-s} \|g(\boldsymbol{\omega}_i \cdot)\|_{s,\Omega} \quad \forall s > 1.$$

Some numerical values of the function m are given at the beginning of section 5.

Using the quadrature (3.3), we can discretize (2.5) in angular direction to get

$$(3.7) \quad \boldsymbol{\omega}_l \cdot \nabla u^l + \sigma_t u^l = \sigma_s \sum_{i=1}^L w_i g(\cdot, \boldsymbol{\omega}_l \cdot \boldsymbol{\omega}_i) u^i + f_l \text{ in } X, \quad u^l = 0 \text{ on } \partial X_-^l, \quad 1 \leq l \leq L,$$

where $f_l = f(\mathbf{x}, \boldsymbol{\omega}_l)$ and $u^l = u^l(\mathbf{x})$ is an approximation of $u(\mathbf{x}, \boldsymbol{\omega}_l)$. Here and below, we use the simplified notation $\partial X_\pm^l := \partial X_{\boldsymbol{\omega}_l, \pm}$.

The system (3.7) is a first-order hyperbolic problem in space, which will be further discretized by the DG method, following [9, 10, 15]. For ease of presentation, we assume X is a polyhedron. Let $\{\mathcal{T}_h\}_{h>0}$ be a regular family of triangulations of X into tetrahedral elements (cf. [6, 8, 13]); $h_K := \text{diam}(K)$ and $h := \max_{K \in \mathcal{T}_h} h_K$. Denote by \mathbf{n}_K the unit outward normal to ∂K for $K \in \mathcal{T}_h$. Let \mathcal{E}_h^i be the set of all interior faces of \mathcal{T}_h . Moreover, with each $e \in \mathcal{E}_h^i$ we associate a unit normal direction \mathbf{n}_e . Associated with the triangulation \mathcal{T}_h , define a finite element space by

$$V_h = \{v \in L^2(\Omega); v|_K \in P_k(K) \forall K \in \mathcal{T}_h\},$$

where k is a nonnegative integer and $P_k(K)$ denotes the set of all polynomials on K of a total degree no more than k . Define $\mathbf{V}_h = (V_h)^L$, and write a generic element in \mathbf{V}_h as $\mathbf{v}_h := \{v_h^l\}_{l=1}^L$ or simply $\mathbf{v}_h := \{v_h^l\}$.

Multiply the first equation of (3.7) by an arbitrary function $v_K \in P_k(K)$ and integrate over K :

$$\int_K \boldsymbol{\omega}_l \cdot \nabla u^l v_K dx + \int_K \sigma_t u^l v_K dx = \int_K \sigma_s \sum_{\substack{i=1 \\ 1 \leq l \leq L}}^L w_i g(\cdot, \boldsymbol{\omega}_l \cdot \boldsymbol{\omega}_i) u^i v_K dx + \int_K f_l v_K dx,$$

which can be reformulated as

$$(3.8) \quad \begin{aligned} & \int_{\partial K} \boldsymbol{\omega}_l \cdot \mathbf{n}_K u^l v_K d\sigma(\mathbf{x}) - \int_K u^l \boldsymbol{\omega}_l \cdot \nabla v_K dx + \int_K \sigma_t u^l v_K dx \\ &= \int_K \sigma_s \sum_{i=1}^L w_i g(\cdot, \boldsymbol{\omega}_l \cdot \boldsymbol{\omega}_i) u^i v_K dx + \int_K f_l v_K dx, \quad 1 \leq l \leq L, \end{aligned}$$

after an integration by parts. We then define the numerical solution $\mathbf{u}_h := \{u_h^l\} \in \mathbf{V}_h$ by requiring

$$(3.9) \quad \begin{aligned} & \int_{\partial K} \boldsymbol{\omega}_l \cdot \mathbf{n}_K \hat{u}_h^l v_K d\sigma(\mathbf{x}) - \int_K u_h^l \boldsymbol{\omega}_l \cdot \nabla v_K dx + \int_K \sigma_t u_h^l v_K dx \\ &= \int_K \sigma_s \sum_{i=1}^L w_i g(\cdot, \boldsymbol{\omega}_l \cdot \boldsymbol{\omega}_i) u_h^i v_K dx + \int_K f_l v_K dx \quad \forall v_K \in P_k(K), \quad 1 \leq l \leq L. \end{aligned}$$

Here, the numerical trace \hat{u}_h^l is defined by the formula

$$(3.10) \quad \hat{u}_h^l(\mathbf{x}) = \begin{cases} 0 & \text{if } (\mathbf{x}, \boldsymbol{\omega}_l) \in \Gamma_-, \\ \lim_{\varepsilon \rightarrow 0+} u_h^l(\mathbf{x} - \varepsilon \boldsymbol{\omega}_l) & \text{otherwise.} \end{cases}$$

The global formulation of the discrete method (3.9) can be expressed as

$$(3.11) \quad \sum_{l=1}^L w_l \sum_{K \in \mathcal{T}_h} \left\{ \int_{\partial K} \boldsymbol{\omega}_l \cdot \mathbf{n}_K \hat{u}_h^l v_{h,K}^l d\sigma(\mathbf{x}) - \int_K u_h^l \boldsymbol{\omega}_l \cdot \nabla v_{h,K}^l dx + \int_K \sigma_t u_h^l v_{h,K}^l dx \right\} \\ - \sum_{l=1}^L w_l \int_X \sigma_s \sum_{i=1}^L w_i g(\cdot, \boldsymbol{\omega}_l \cdot \boldsymbol{\omega}_i) u_h^i v_h^l dx = \sum_{l=1}^L w_l \int_X f_l v_h^l dx \quad \forall \mathbf{v}_h = \{v_h^l\} \in \mathbf{V}_h,$$

where $v_{h,K}^l := v_h^l|_K$ for all $v_h^l \in V_h$. For all $\mathbf{u}_h, \mathbf{v}_h \in \mathbf{V}_h$, define

$$(3.12) \quad a_h^{(1)}(\mathbf{u}_h, \mathbf{v}_h) = \sum_{l=1}^L w_l \sum_{K \in \mathcal{T}_h} \left\{ \int_{\partial K} \boldsymbol{\omega}_l \cdot \mathbf{n}_K \hat{u}_h^l v_{h,K}^l d\sigma(\mathbf{x}) \right. \\ \left. - \int_K u_h^l \boldsymbol{\omega}_l \cdot \nabla v_{h,K}^l dx + \int_K \sigma_t u_h^l v_{h,K}^l dx \right\} \\ - \sum_{l=1}^L w_l \int_X \sigma_s \sum_{i=1}^L w_i g(\cdot, \boldsymbol{\omega}_l \cdot \boldsymbol{\omega}_i) u_h^i v_h^l dx,$$

$$(3.13) \quad f(\mathbf{v}_h) = \sum_{l=1}^L w_l \int_X f_l v_h^l dx.$$

Then, the discrete-ordinate DG method (3.11) (or equivalently (3.9)) can be recast as follows.

Find $\mathbf{u}_h \in \mathbf{V}_h$ such that

$$(3.14) \quad a_h^{(1)}(\mathbf{u}_h, \mathbf{v}_h) = f(\mathbf{v}_h) \quad \forall \mathbf{v}_h \in \mathbf{V}_h.$$

As pointed out in [9,10], when solving hyperbolic problems by DG methods, it is preferable to add some stabilization terms in the DG scheme to penalize the jump of the solution across interior faces of the triangulation, in order to avoid nonphysical oscillations in the numerical solution due to discontinuities in the data. For this purpose, we need some additional notation. For an interior face $e \in \mathcal{E}_h^i$, let K^+ and K^- be two adjacent tetrahedrons sharing e , with the unit direction \mathbf{n}_e given before pointing from K^- to K^+ . For a scalar-valued function v , write $v^+ = v|_{K^+}$ and $v^- = v|_{K^-}$. Then define the jump of v on e by $[v] = v^+ - v^-$. Now, we can define the following discrete-ordinate DG method with stabilization:

Find $\mathbf{u}_h \in \mathbf{V}_h$ such that

$$(3.15) \quad a_h^{(2)}(\mathbf{u}_h, \mathbf{v}_h) = f(\mathbf{v}_h) \quad \forall \mathbf{v}_h \in \mathbf{V}_h,$$

where

$$(3.16) \quad a_h^{(2)}(\mathbf{u}_h, \mathbf{v}_h) := a_h^{(1)}(\mathbf{u}_h, \mathbf{v}_h) + c_p \sum_{l=1}^L w_l \sum_{e \in \mathcal{E}_h^i} \int_e [u_h^l] [v_h^l] d\sigma(\mathbf{x}),$$

with $a_h^{(1)}(\cdot, \cdot)$ given by (3.12) and $c_p > 0$ a penalty parameter. As we will see from Lemma 4.4 in section 4, the bilinear form $a^{(2)}(\cdot, \cdot)$ has a stronger stability property than $a^{(1)}(\cdot, \cdot)$. In section 5, we will see some numerical results for the influence of the value of c_p on the solution accuracy.

4. Error analysis. We first give a simple but useful lemma for error analysis of the numerical methods, which is similar to the second Strang lemma in error analysis of nonconforming element methods (cf. [13]).

LEMMA 4.1. *Let $\{W_h\}_{h>0}$ be a family of finite-dimensional spaces equipped with norms $\{\|\cdot\|_h\}_{h>0}$. Let $b_h(\cdot, \cdot)$ be a uniformly coercive bilinear form over W_h , i.e., there exists a positive constant α independent of h such that*

$$(4.1) \quad \alpha \|w_h\|_h^2 \leq b_h(w_h, w_h) \quad \forall w_h \in W_h.$$

Assume v is a function such that $b_h(v, w_h)$ is well defined for all $w_h \in W_h$, and v_h is a function in W_h satisfying

$$(4.2) \quad b_h(v - v_h, w_h) = 0 \quad \forall w_h \in W_h.$$

Then

$$(4.3) \quad \|v - v_h\|_h \leq \inf_{w_h \in W_h} \left\{ \|v - w_h\|_h + \frac{1}{\alpha} \sup_{\bar{w}_h \in \bar{W}_h} \frac{b_h(v - w_h, \bar{w}_h)}{\|\bar{w}_h\|_h} \right\}.$$

Proof. For any $w_h \in W_h$, it follows from the triangle inequality that

$$(4.4) \quad \|v - v_h\|_h \leq \|v - w_h\|_h + \|w_h - v_h\|_h.$$

From (4.1) and (4.2) we find

$$\alpha \|w_h - v_h\|_h^2 \leq b_h(w_h - v_h, w_h - v_h) = b_h(w_h - v, w_h - v_h),$$

which implies, for $w_h \neq v_h$,

$$\|w_h - v_h\|_h \leq \frac{1}{\alpha} \frac{b_h(w_h - v, w_h - v_h)}{\|w_h - v_h\|_h} \leq \frac{1}{\alpha} \sup_{\bar{w}_h \in \bar{W}_h} \frac{b_h(v - w_h, \bar{w}_h)}{\|\bar{w}_h\|_h}.$$

This, together with (4.4), leads to the estimate (4.3). \square

For any $K \in \mathcal{T}_h$, let P_K be the $L^2(K)$ -orthogonal projection operator from $L^2(K)$ onto $P_k(K)$. Then by the scaling argument and the trace theorem we can easily obtain the following result (cf. [6, 8, 13]).

LEMMA 4.2. *For all $v \in H^r(K)$ with $r > 0$ and $K \in \mathcal{T}_h$,*

$$\|v - P_K v\|_{0,K} + h_K^{1/2} \|v - P_K v\|_{0,\partial K} \lesssim h_K^{\min\{r, k+1\}} \|v\|_{r,K}.$$

We will need the following result on several occasions.

LEMMA 4.3. *For all $\mathbf{v} := \{v^l\}$, $\mathbf{w} := \{w^l\} \in (L^2(\Omega))^L$,*

$$\begin{aligned} & \sum_{l=1}^L w_l \int_X \sigma_s \sum_{i=1}^L w_i g(\cdot, \boldsymbol{\omega}_l \cdot \boldsymbol{\omega}_i) v^i w^l dx \\ & \leq \left[\sum_{l=1}^L w_l \int_X m \sigma_s (v^l)^2 dx \right]^{1/2} \left[\sum_{l=1}^L w_l \int_X m \sigma_s (w^l)^2 dx \right]^{1/2}. \end{aligned}$$

Proof. Denote the left side of the inequality by I. Interchanging the order of summation and using the Cauchy–Schwarz inequality, we find

(4.5)

$$\begin{aligned} I &= \sum_{i=1}^L w_i \sum_{l=1}^L w_l \int_X \sigma_s g(\cdot, \omega_l \cdot \omega_i) v^i w^l dx \\ &\leq \sum_{i=1}^L w_i \left[\sum_{l=1}^L w_l \int_X \sigma_s g(\cdot, \omega_l \cdot \omega_i) (v^i)^2 dx \right]^{1/2} \left[\sum_{l=1}^L w_l \int_X \sigma_s g(\cdot, \omega_l \cdot \omega_i) (w^l)^2 dx \right]^{1/2}. \end{aligned}$$

By the definition (3.5), it is easy to know

$$\sum_{l=1}^L w_l \int_X \sigma_s g(\cdot, \omega_l \cdot \omega_i) (v^i)^2 dx \leq \int_X m \sigma_s (v^i)^2 dx.$$

Therefore, a combination of estimate (4.5) and the Cauchy–Schwarz inequality leads to

$$\begin{aligned} I &\leq \sum_{i=1}^L w_i \left[\int_X m \sigma_s (v^i)^2 dx \right]^{1/2} \left[\sum_{l=1}^L w_l \int_X \sigma_s g(\cdot, \omega_l \cdot \omega_i) (w^l)^2 dx \right]^{1/2} \\ &\leq \left[\sum_{i=1}^L w_i \int_X m \sigma_s (v^i)^2 dx \right]^{1/2} \left[\sum_{l,i=1}^L w_i w_l \int_X \sigma_s g(\cdot, \omega_l \cdot \omega_i) (w^l)^2 dx \right]^{1/2} \\ &\leq \left[\sum_{l=1}^L w_l \int_X m \sigma_s (v^l)^2 dx \right]^{1/2} \left[\sum_{l=1}^L w_l \int_X m \sigma_s (w^l)^2 dx \right]^{1/2}, \end{aligned}$$

as desired. \square

To derive stability bounds for the methods (3.14) and (3.15), we define norms $\|\cdot\|_h^{(1)}$ and $\|\cdot\|_h^{(2)}$ over \mathbf{V}_h by

(4.6)

$$\|\mathbf{v}\|_h^{(1)} = \left[\sum_{l=1}^L w_l \left(\|v^l\|_{0,X}^2 + \sum_{e \in \mathcal{E}_h^i} \int_e |\omega_l \cdot \mathbf{n}_e| |[v^l]|^2 d\sigma(\mathbf{x}) + \int_{\partial X_+^l} \omega_l \cdot \mathbf{n} |v^l|^2 d\sigma(\mathbf{x}) \right) \right]^{1/2},$$

(4.7)

$$\|\mathbf{v}\|_h^{(2)} = \left[\sum_{l=1}^L w_l \left(\|v^l\|_{0,X}^2 + c_p \sum_{e \in \mathcal{E}_h^i} \int_e |[v^l]|^2 d\sigma(\mathbf{x}) + \int_{\partial X_+^l} \omega_l \cdot \mathbf{n} |v^l|^2 d\sigma(\mathbf{x}) \right) \right]^{1/2}$$

for all $\mathbf{v} \in \mathbf{V}_h$. These norms can be applied to any function $\mathbf{v} = \{v^l\}_{l=1}^L$ for which all the right-side terms make sense. We have the following stability estimates.

LEMMA 4.4 (stability). *Under the assumption (3.6),*

$$(4.8) \quad (\|\mathbf{v}_h\|_h^{(1)})^2 \lesssim a_h^{(1)}(\mathbf{v}_h, \mathbf{v}_h), \quad (\|\mathbf{v}_h\|_h^{(2)})^2 \lesssim a_h^{(2)}(\mathbf{v}_h, \mathbf{v}_h) \quad \forall \mathbf{v}_h \in \mathbf{V}_h.$$

Proof. It suffices to prove the first estimate in (4.8), since the second estimate follows directly from the first one and the definition (4.7). For any $\mathbf{v}_h = \{v_h^l\} \in \mathbf{V}_h$,

we have by the definition (3.12) that

$$(4.9) \quad a_h^{(1)}(\mathbf{v}_h, \mathbf{v}_h) = I_1 + I_2,$$

where

$$\begin{aligned} I_1 &:= \sum_{l=1}^L w_l \sum_{K \in \mathcal{T}_h} \left\{ \int_{\partial K} \boldsymbol{\omega}_l \cdot \mathbf{n}_K \hat{v}_h^l v_{h,K}^l d\sigma(\mathbf{x}) - \int_K v_h^l \boldsymbol{\omega}_l \cdot \nabla v_{h,K}^l dx \right\}, \\ I_2 &:= \sum_{l=1}^L w_l \int_X \sigma_t(v_h^l)^2 dx - \sum_{l=1}^L w_l \int_X \sigma_s \sum_{i=1}^L w_i g(\cdot, \boldsymbol{\omega}_l \cdot \boldsymbol{\omega}_i) v_h^i v_h^l dx. \end{aligned}$$

It follows from Lemma 4.3 and (3.6) that

$$(4.10) \quad I_2 \geq \sum_{l=1}^L w_l \int_X (\sigma_t - m\sigma_s)(v_h^l)^2 dx \geq c'_0 \sum_{l=1}^L w_l \int_X (v_h^l)^2 dx.$$

For a lower bound of I_1 , we first perform an integration by parts to obtain

$$\begin{aligned} &\int_{\partial K} \boldsymbol{\omega}_l \cdot \mathbf{n}_K \hat{v}_h^l v_{h,K}^l d\sigma(\mathbf{x}) - \int_K v_h^l \boldsymbol{\omega}_l \cdot \nabla v_{h,K}^l dx \\ &= \int_{\partial K} \boldsymbol{\omega}_l \cdot \mathbf{n}_K \hat{v}_h^l v_{h,K}^l d\sigma(\mathbf{x}) - \frac{1}{2} \int_K \boldsymbol{\omega}_l \cdot \nabla (v_h^l)^2 dx \\ &= \int_{\partial K} \boldsymbol{\omega}_l \cdot \mathbf{n}_K \hat{v}_h^l v_{h,K}^l d\sigma(\mathbf{x}) - \frac{1}{2} \int_{\partial K} \boldsymbol{\omega}_l \cdot \mathbf{n}_K (v_h^l)^2 d\sigma(\mathbf{x}) \\ &= \frac{1}{2} \int_{\partial K} \boldsymbol{\omega}_l \cdot \mathbf{n}_K [(\hat{v}_h^l)^2 - (v_h^l - \hat{v}_h^l)^2] d\sigma(\mathbf{x}). \end{aligned}$$

Due to the choice of \hat{v}_h^l , (3.10), we know that $\hat{v}_h^l = v_h^l$ on ∂X_+^l , $\hat{v}_h^l = 0$ on ∂X_-^l , and on ∂K , if $\boldsymbol{\omega}_l \cdot \mathbf{n}_K \geq 0$, then $\hat{v}_h^l(\mathbf{x}) = v_h^l(\mathbf{x})$. Therefore, multiplying by w_l in the above equation and then summing over all $K \in \mathcal{T}_h$ and $1 \leq l \leq L$, we find

$$\begin{aligned} (4.11) \quad I_1 &= \frac{1}{2} \sum_{l=1}^L w_l \sum_{K \in \mathcal{T}_h} \int_{\partial K} \boldsymbol{\omega}_l \cdot \mathbf{n}_K (\hat{v}_h^l)^2 d\sigma(\mathbf{x}) + \frac{1}{2} \sum_{l=1}^L w_l \sum_{K \in \mathcal{T}_h} \int_{\partial K} |\boldsymbol{\omega}_l \cdot \mathbf{n}_K| (v_h^l - \hat{v}_h^l)^2 d\sigma(\mathbf{x}) \\ &= \frac{1}{2} \sum_{l=1}^L w_l \int_{\partial X_+^l} \boldsymbol{\omega}_l \cdot \mathbf{n} (v_h^l)^2 d\sigma(\mathbf{x}) + \frac{1}{2} \sum_{l=1}^L w_l \sum_{K \in \mathcal{T}_h} \int_{\partial K} |\boldsymbol{\omega}_l \cdot \mathbf{n}_K| (v_h^l - \hat{v}_h^l)^2 d\sigma(\mathbf{x}) \\ &\geq \frac{1}{2} \sum_{l=1}^L w_l \int_{\partial X_+^l} \boldsymbol{\omega}_l \cdot \mathbf{n} (v_h^l)^2 d\sigma(\mathbf{x}) + \frac{1}{2} \sum_{l=1}^L w_l \sum_{e \in \mathcal{E}_h^i} \int_e |\boldsymbol{\omega}_l \cdot \mathbf{n}_e| |[v^l]|^2 d\sigma(\mathbf{x}). \end{aligned}$$

The first estimate of (4.8) follows from (4.9)–(4.11). \square

The following result is a direct consequence of the above lemma.

THEOREM 4.5. *Under the assumption (3.6), both discrete-ordinate DG methods (3.14) and (3.15) have a unique solution.*

Now, we are ready to give error estimates for the methods (3.14) and (3.15). For this purpose, we make a regularity assumption:

$$(4.12) \quad \text{for some } r > 0, u^l \in H^r(X), 1 \leq l \leq L.$$

THEOREM 4.6. *Under the assumptions (3.6) and (4.12), the discrete-ordinate DG method (3.14) admits the following error estimate:*

$$\| \{u^l\} - \mathbf{u}_h \|_h^{(1)} \lesssim h^{\min\{r,k+1\}-1/2} \left(\sum_{l=1}^L w_l \|u^l\|_{r,X}^2 \right)^{1/2}.$$

Proof. By (3.8) and the definitions (3.12)–(3.13), we have

$$a_h^{(1)}(\{u^l\}, \mathbf{v}_h) = f(\mathbf{v}_h) \quad \forall \mathbf{v}_h \in V_h.$$

Subtract (3.14) from the above equality to obtain the Galerkin orthogonality

$$a_h^{(1)}(\{u^l\} - \mathbf{u}_h, \mathbf{v}_h) = 0 \quad \forall \mathbf{v}_h \in V_h.$$

Therefore, it follows from the first estimate of (4.8) and Lemma 4.1 that

$$(4.13) \quad \| \{u^l\} - \mathbf{u}_h \|_h^{(1)} \leq \| \{u^l\} - \{P_h u^l\} \|_h^{(1)} + \sup_{\mathbf{v}_h \in V_h} \frac{a_h^{(1)}(\{u^l\} - \{P_h u^l\}, \mathbf{v}_h)}{\| \mathbf{v}_h \|_h^{(1)}},$$

where P_h denotes the L^2 -orthogonal operator onto V_h in an elementwise way, i.e., for $v \in L^2(X)$, $P_h v|_K := P_K v$. By Lemma 4.2 and the definition of $\| \cdot \|_h^{(1)}$, we know

$$\begin{aligned} & (\| \{u^l\} - \{P_h u^l\} \|_h^{(1)})^2 \\ & \lesssim \sum_{l=1}^L w_l \|u^l - P_h u^l\|_{0,X}^2 + \sum_{l=1}^L w_l \sum_{e \in \mathcal{E}_h^i} \int_e |[u^l - P_h u^l]|^2 d\sigma(\mathbf{x}) \\ & \quad + \sum_{l=1}^L w_l \int_{\partial X_+^l} |u^l - P_h u^l|^2 d\sigma(\mathbf{x}) \\ & \lesssim \sum_{l=1}^L w_l \sum_{K \in \mathcal{T}_h} \|u_K^l - P_K u_K^l\|_{0,K}^2 + \sum_{l=1}^L w_l \sum_{K \in \mathcal{T}_h} \|u_K^l - P_K u_K^l\|_{0,\partial K}^2 \\ & \lesssim \sum_{l=1}^L w_l \sum_{K \in \mathcal{T}_h} h_K^{2\min\{r,k+1\}} \|u_K^l\|_{r,K}^2 + \sum_{l=1}^L w_l \sum_{K \in \mathcal{T}_h} h_K^{2\min\{r,k+1\}-1} \|u_K^l\|_{r,K}^2 \\ & \lesssim h^{2\min\{r,k+1\}-1} \sum_{l=1}^L w_l \|u^l\|_{r,X}^2, \end{aligned}$$

i.e.,

$$(4.14) \quad \| \{u^l\} - \{P_h u^l\} \|_h^{(1)} \lesssim h^{\min\{r,k+1\}-1/2} \left(\sum_{l=1}^L w_l \|u^l\|_{r,X}^2 \right)^{1/2}.$$

On the other hand, by the definition of $a_h(\cdot, \cdot)$, we have

$$(4.15) \quad a_h^{(1)}(\{u^l\} - \{P_h u^l\}, \mathbf{v}_h) = \mathbb{I}_1 + \mathbb{I}_2,$$

where

$$\begin{aligned}\mathbb{I}_1 &:= \sum_{l=1}^L w_l \sum_{K \in \mathcal{T}_h} \left\{ \int_{\partial K} \boldsymbol{\omega}_l \cdot \mathbf{n}_K (\widehat{u^l - P_h u^l}) v_{h,K}^l d\sigma(\mathbf{x}) - \int_K (u_K^l - P_K u_K^l) \boldsymbol{\omega}_l \cdot \nabla v_{h,K}^l dx \right\}, \\ \mathbb{I}_2 &:= \sum_{l=1}^L w_l \int_X \sigma_t (u^l - P_h u^l) v_h^l dx - \sum_{l=1}^L w_l \int_X \sigma_s \sum_{i=1}^L w_i g(\cdot, \boldsymbol{\omega}_l \cdot \boldsymbol{\omega}_i) (u^i - P_h u^i) v_h^l dx.\end{aligned}$$

Since $\boldsymbol{\omega}_l \cdot \nabla v_{h,K}^l \in P_k(K)$, we know

$$\int_K (u_K^l - P_K u_K^l) \boldsymbol{\omega}_l \cdot \nabla v_{h,K}^l dx = 0.$$

For each l between 1 and L , denote by $\mathcal{E}_h^{l,+}$ the set of all faces of \mathcal{T}_h on ∂X_+^l . Using the Cauchy–Schwarz inequality and Lemma 4.2, we have

(4.16)

$$\begin{aligned}|\mathbb{I}_1| &\lesssim \sum_{l=1}^L w_l \sum_{e \in \mathcal{E}_h^{l,+}} \int_e \boldsymbol{\omega}_l \cdot \mathbf{n} |u^l - P_h u^l| |v_h^l| d\sigma(\mathbf{x}) \\ &\quad + \sum_{l=1}^L w_l \sum_{e \in \mathcal{E}_h^i} \int_e |\boldsymbol{\omega}_l \cdot \mathbf{n}_e| |u^l - P_h u^l| |[v_h^l]| d\sigma(\mathbf{x}) \\ &\lesssim \sum_{l=1}^L w_l \left[\sum_{e \in \mathcal{E}_h^{l,+}} \int_e |u^l - P_h u^l|^2 d\sigma(\mathbf{x}) \right]^{1/2} \left[\sum_{e \in \mathcal{E}_h^{l,+}} \int_e \boldsymbol{\omega}_l \cdot \mathbf{n} |v_h^l|^2 d\sigma(\mathbf{x}) \right]^{1/2} \\ &\quad + \sum_{l=1}^L w_l \left[\sum_{e \in \mathcal{E}_h^i} \int_e |u^l - P_h u^l|^2 d\sigma(\mathbf{x}) \right]^{1/2} \left[\sum_{e \in \mathcal{E}_h^i} \int_e |\boldsymbol{\omega}_l \cdot \mathbf{n}_e| |[v_h^l]|^2 d\sigma(\mathbf{x}) \right]^{1/2} \\ &\lesssim h^{\min\{r, k+1\}-1/2} \left(\sum_{l=1}^L w_l \|u^l\|_{r,X}^2 \right)^{1/2} |||\mathbf{v}_h|||_h^{(1)}.\end{aligned}$$

From Lemmas 4.2, 4.3, and the Cauchy–Schwarz inequality, it follows that

$$\begin{aligned}|\mathbb{I}_2| &\lesssim \left[\sum_{l=1}^L w_l \int_X (u^l - P_h u^l)^2 dx \right]^{1/2} \left[\sum_{l=1}^L w_l \int_X (v_h^l)^2 dx \right]^{1/2} \\ &\lesssim h^{\min\{r, k+1\}-1/2} \left(\sum_{l=1}^L w_l \|u^l\|_{r,X}^2 \right)^{1/2} |||\mathbf{v}_h|||_h^{(1)}.\end{aligned}$$

This, together with (4.13)–(4.16), leads to the stated error estimate. \square

Applying a similar argument as in the proof of the above theorem, we can also derive an error estimate for the method (3.15).

THEOREM 4.7. *Under the assumptions (3.6) and (4.12), the discrete-ordinate DG method (3.15) admits the following error estimate:*

$$|||\{u^l\} - \mathbf{u}_h|||_h^{(2)} \lesssim (1 + \sqrt{c_p}) h^{\min\{r, k+1\}-1/2} \left(\sum_{l=1}^L w_l \|u^l\|_{r,X}^2 \right)^{1/2}.$$

Now, we proceed with bounding the errors $\varepsilon^l(\mathbf{x}) := u(\mathbf{x}, \boldsymbol{\omega}_l) - u^l(\mathbf{x})$, $1 \leq l \leq L$, arising from the semidiscretization (3.7). First, it follows from (2.5) and (3.7) that, for all $1 \leq l \leq L$,

$$(4.17) \quad \begin{aligned} \boldsymbol{\omega}_l \cdot \nabla \varepsilon^l + \sigma_t \varepsilon^l &= \sigma_s \int_{\Omega} g(\cdot, \boldsymbol{\omega}_l \cdot \boldsymbol{\omega}) u(\cdot, \boldsymbol{\omega}) d\sigma(\boldsymbol{\omega}) - \sigma_s \sum_{i=1}^L w_i g(\cdot, \boldsymbol{\omega}_l \cdot \boldsymbol{\omega}_i) u^i \\ &= \sigma_s \sum_{i=1}^L w_i g(\cdot, \boldsymbol{\omega}_l \cdot \boldsymbol{\omega}_i) \varepsilon^i + \eta^l, \end{aligned}$$

where

$$(4.18) \quad \eta^l := \sigma_s \int_{\Omega} g(\cdot, \boldsymbol{\omega}_l \cdot \boldsymbol{\omega}) u(\cdot, \boldsymbol{\omega}) d\sigma(\boldsymbol{\omega}) - \sigma_s \sum_{i=1}^L w_i g(\cdot, \boldsymbol{\omega}_l \cdot \boldsymbol{\omega}_i) u(\cdot, \boldsymbol{\omega}_i).$$

Multiplying (4.17) by $w_l \varepsilon^l$, integrating over X , and summing over $1 \leq l \leq L$, we have by the Stokes theorem that

$$\begin{aligned} \frac{1}{2} \sum_{l=1}^L w_l \int_{\partial X_+^l} \boldsymbol{\omega}_l \cdot \mathbf{n} (\varepsilon^l)^2 d\sigma(\mathbf{x}) + \sum_{l=1}^L w_l \int_X \sigma_t (\varepsilon^l)^2 dx \\ - \sum_{l=1}^L w_l \int_X \sigma_s \sum_{i=1}^L w_i g(\cdot, \boldsymbol{\omega}_l \cdot \boldsymbol{\omega}_i) \varepsilon^i \varepsilon^l dx = \sum_{l=1}^L w_l \int_X \varepsilon^l \eta^l dx. \end{aligned}$$

Applying to the above equation an argument similar to that leading to (4.10), we obtain

$$c'_0 \sum_{l=1}^L w_l \int_X (\varepsilon^l)^2 dx \leq \sum_{l=1}^L w_l \int_X \varepsilon^l \eta^l dx.$$

Then apply the Cauchy–Schwarz inequality to obtain

$$(4.19) \quad \sum_{l=1}^L w_l \int_X (\varepsilon^l)^2 dx \lesssim \sum_{l=1}^L w_l \int_X (\eta^l)^2 dx.$$

Assume

$$(4.20) \quad \text{for some } r' > 1, \quad \sup_{\mathbf{x} \in X, \boldsymbol{\omega} \in \Omega} \|g(\mathbf{x}, \boldsymbol{\omega} \cdot)\|_{r', \Omega} < \infty, \quad u \in L^2(X, H^{r'}(\Omega)).$$

Note that for the Henyey–Greenstein phase function, the above assumption on g is satisfied for any $r' > 1$. Then, applying (3.4),

$$\begin{aligned} |\eta^l(\mathbf{x})| &= \sigma_s(\mathbf{x}) \left| \int_{\Omega} g(\cdot, \boldsymbol{\omega}_l \cdot \boldsymbol{\omega}) u(\mathbf{x}, \boldsymbol{\omega}) d\sigma(\boldsymbol{\omega}) - \sum_{i=1}^L w_i g(\cdot, \boldsymbol{\omega}_l \cdot \boldsymbol{\omega}_i) u(\mathbf{x}, \boldsymbol{\omega}_i) \right| \\ &\lesssim c(r') n^{-r'} \|g(\mathbf{x}, \boldsymbol{\omega}_l \cdot) u(\mathbf{x}, \cdot)\|_{r', \Omega} \lesssim c(r') n^{-r'} \|g(\mathbf{x}, \boldsymbol{\omega}_l \cdot)\|_{r', \Omega} \|u(\mathbf{x}, \cdot)\|_{r', \Omega}, \end{aligned}$$

where $c(r')$ is a positive constant depending only on r' . Collecting the last two estimates gives

$$\sum_{l=1}^L w_l \int_X (\varepsilon^l)^2 dx \lesssim c(r', g)^2 n^{-2r'} \int_X \|u(\mathbf{x}, \cdot)\|_{r', \Omega}^2 dx,$$

where

$$c(r', g) := c(r') \sup_{\boldsymbol{x} \in X, \boldsymbol{\omega} \in \Omega} \|g(\boldsymbol{x}, \boldsymbol{\omega} \cdot)\|_{r', \Omega}.$$

This combined with Theorems 4.6 and 4.7 leads to the following result, for bounds on the error

$$(4.21) \quad \|u - u_h\|_h = \left(\sum_{l=1}^L w_l \|u(\cdot, \boldsymbol{\omega}_l) - u_h^l\|_{0,X}^2 \right)^{1/2}.$$

COROLLARY 4.8. *Let n be the degree of precision of the numerical quadrature (3.1). Assume (3.6), (4.12), and (4.20). Then for the discrete-ordinate DG method (3.14), we have*

$$\|u - u_h\|_h \lesssim h^{\min\{r, k+1\}-1/2} \left(\sum_{l=1}^L w_l \|u^l\|_{r,X}^2 \right)^{1/2} + c(r', g) n^{-r'} \left(\int_X \|u(\cdot, \cdot)\|_{r', \Omega}^2 dx \right)^{1/2},$$

and for the discrete-ordinate DG method (3.15),

$$\begin{aligned} \|u - u_h\|_h &\lesssim (1 + \sqrt{c_p}) h^{\min\{r, k+1\}-1/2} \left(\sum_{l=1}^L w_l \|u^l\|_{r,X}^2 \right)^{1/2} \\ &\quad + c(r', g) n^{-r'} \left(\int_X \|u(\cdot, \cdot)\|_{r', \Omega}^2 dx \right)^{1/2}. \end{aligned}$$

5. Numerical results. We first return to the assumption (3.6). Recalling the normalization condition (2.3), we expect that as long as the numerical quadrature (3.2) is sufficiently accurate, the quantity $m(\boldsymbol{x})$ defined in (3.5) will be close to 1, and then the assumption (3.6) will follow from the condition (2.7). As an example, for the Henyey–Greenstein phase function, consider using the S_N quadratures for the numerical integration (cf. [11]). Note that $m = m(\boldsymbol{x})$ does not depend on \boldsymbol{x} . Due to the symmetry of the S_N quadratures, it is easy to see that for any $\eta \in (-1, 1)$, the value of m corresponding to η equals that corresponding to $-\eta$. Also, note that $m = 1$ for $\eta = 0$. In Table 5.1, we list the value of m for $\eta = 0.2, 0.4, 0.6, 0.8$, and a few choices of N .

We then present several numerical examples in solving the boundary value problem (2.5)–(2.6). The main purpose is to illustrate the performance of the proposed methods, especially on numerical convergence orders. For the angular variable $\boldsymbol{\omega}$, we will write both $\boldsymbol{\omega} = (\omega_1, \omega_2, \omega_3)^T$ and $\boldsymbol{\omega} = (\sin \theta \cos \psi, \sin \theta \sin \psi, \cos \theta)^T$, and for the spatial variable, $\boldsymbol{x} = (x_1, x_2, x_3)^T$. We use the Henyey–Greenstein phase function

TABLE 5.1
Value of m for several choices of η and N .

	$\eta = 0.2$	$\eta = 0.4$	$\eta = 0.6$	$\eta = 0.8$
$N = 2$	1.004065	1.082299	1.627474	5.790811
$N = 4$	1.000013	1.002545	1.073823	2.216768
$N = 6$	1.000001	1.000355	1.016232	1.476457
$N = 8$	1.000000	1.000028	1.004487	1.249246
$N = 12$	1.000000	1.000001	1.000500	1.083949
$N = 16$	0.999999	1.000000	1.000082	1.033950

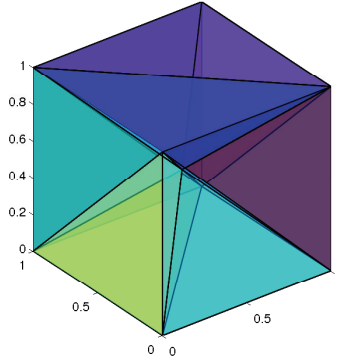


FIG. 5.1. A sample mesh.

defined in (2.4) with constant cross sections $\sigma_t(\mathbf{x}) = \sigma_t$ and $\sigma_s(\mathbf{x}) = \sigma_s$. We will report numerical values of the error $\|u - u_h\|_h$, defined by (4.6) for $c_p = 0$ and by (4.7) for $c_p > 0$, as well as the error $\|u - u_h\|_h$ defined in (4.21).

The spatial domain is $X = (0, 1)^3$. For a positive integer n , we partition \overline{X} into n^3 subcubes $\{X_i\}$, each with edge length $1/n$. Denote by S the set of all the centers and vertices of the subcubes. A mesh is generated by creating the Delaunay tessellation of the points in S . This is accomplished by using the *delaunay3* algorithm in MATLAB. The option “QJ” is passed to *delaunay3* to ensure no hanging nodes are created. Denote by h the maximum length of the edges of the tetrahedron in the mesh; $h = \sqrt{2}/n$. A sample mesh (for $n = 1$) is shown in Figure 5.1. The local polynomial degree $k = 1$. In the examples, if not stated otherwise, we use the S_4 quadrature for the integration on the unit sphere so that there are 24 different angular directions $\{\omega_l\}_{l=1}^{24}$. In some of the examples, we use the more accurate S_{12} quadrature, and there are 168 different angular directions $\{\omega_l\}_{l=1}^{168}$. The error figures correspond to the parameter $c_p = 0.1$. Some general observations on the numerical results are stated after the examples.

Example 5.1. We take $\sigma_t = 2$, $\sigma_s = 1$, and $\eta = 0$. With the right-hand side function

$$\begin{aligned} f(\mathbf{x}, \boldsymbol{\omega}) = & \pi\omega_1 \cos(\pi x_1) \sin(\pi x_2) \sin(\pi x_3) + \pi\omega_2 \sin(\pi x_1) \cos(\pi x_2) \sin(\pi x_3) \\ & + \pi\omega_3 \sin(\pi x_1) \sin(\pi x_2) \cos(\pi x_3) + \sin(\pi x_1) \sin(\pi x_2) \sin(\pi x_3), \end{aligned}$$

the true solution is

$$u(\mathbf{x}, \boldsymbol{\omega}) = \sin(\pi x_1) \sin(\pi x_2) \sin(\pi x_3).$$

Errors of numerical solutions are shown in Tables 5.2, 5.3, and Figure 5.2.

TABLE 5.2
Error $\|u - u_h\|_h$ for Example 5.1.

h	$c_p = 0$	$c_p = .01$	$c_p = .1$	$c_p = 1$	$c_p = 10$
$\frac{\sqrt{2}}{2}$	0.134053	0.133282	0.131273	0.147883	0.184881
$\frac{\sqrt{2}}{3}$	0.063796	0.063296	0.061977	0.069285	0.079147
$\frac{\sqrt{2}}{5}$	0.024395	0.024158	0.023503	0.025016	0.026554
$\frac{\sqrt{2}}{7}$	0.012750	0.012609	0.012221	0.012746	0.013246
$\frac{\sqrt{2}}{10}$	0.006356	0.006276	0.006067	0.006243	0.006415

TABLE 5.3
Error $\|u - u_h\|_h$ for Example 5.1.

h	$c_p = 0$	$c_p = .01$	$c_p = .1$	$c_p = 1$	$c_p = 10$
$\frac{\sqrt{2}}{2}$	0.401351	0.164141	0.213165	0.280863	0.253321
$\frac{\sqrt{2}}{3}$	0.238294	0.080613	0.114482	0.151232	0.109445
$\frac{\sqrt{2}}{5}$	0.119302	0.032524	0.052300	0.066705	0.040208
$\frac{\sqrt{2}}{7}$	0.074148	0.018049	0.031313	0.039332	0.021865
$\frac{\sqrt{2}}{10}$	0.044332	0.009731	0.018185	0.022612	0.011813

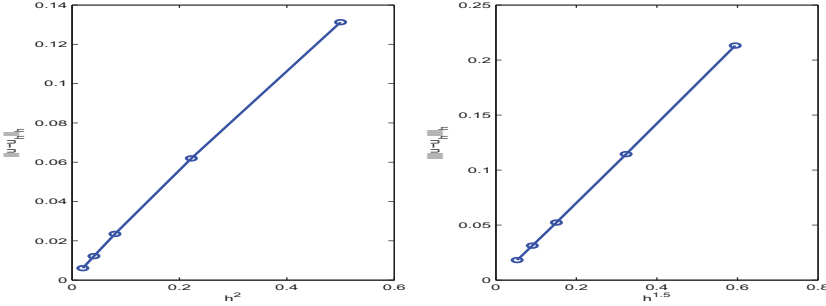


FIG. 5.2. Example 5.1: $\|u - u_h\|_h$ vs. h^2 (left) and $\|u - u_h\|_h$ vs. $h^{1.5}$ (right).

Example 5.2. Let $\eta = 0$. Define an auxiliary function

$$u_1(\mathbf{x}, \theta) = e^{\theta x_1 x_2 x_3 \sin(2\pi x_1) \sin(\pi x_2) \sin(\pi x_3)}.$$

Consider a problem with the right-hand side function

$$\begin{aligned} f(\mathbf{x}, \omega) = & 10\sigma_t [u_1(\mathbf{x}, \theta) - 1] + 5\sigma_s \left[2 - \frac{1 + e^{\pi x_1 x_2 x_3 \sin(2\pi x_1) \sin(\pi x_2) \sin(\pi x_3)}}{1 + x_1^2 x_2^2 x_3^2 \sin^2(2\pi x_1)^2 \sin^2(\pi x_2)^2 \sin^2(\pi x_3)^2} \right] \\ & + 10u_1(\mathbf{x}, \theta) \left\{ \theta x_1 x_2 \cos \theta \sin(2\pi x_1) \sin(\pi x_2) [\pi x_3 \cos(\pi x_3) + \sin(\pi x_3)] \right. \\ & + \theta x_1 x_3 \sin \psi \sin \theta \sin(2\pi x_1) \sin(\pi x_3) [\pi x_2 \cos(\pi x_2) + \sin(\pi x_2)] \\ & \left. + \theta x_2 x_3 \cos \psi \sin \theta \sin(\pi x_2) \sin(\pi x_3) [2\pi x_1 \cos(2\pi x_1) + \sin(2\pi x_1)] \right\}. \end{aligned}$$

The true solution is

$$u(\mathbf{x}, \omega) = 10 [u_1(\mathbf{x}, \theta) - 1].$$

Numerical results for $\sigma_t = 4$ and $\sigma_s = 1$ are reported in Tables 5.4, 5.5, and Figure 5.3.

Example 5.3. In this example we use a nonconstant phase function. Choose the true solution to be

$$u(\mathbf{x}, \omega) = 10\omega_3 \sin(\pi x_1) \sin(\pi x_2) \sin(\pi x_3).$$

The corresponding right-hand side function is

$$\begin{aligned} f(\mathbf{x}, \omega) = & 10 (\sigma_t \omega_3 - \eta \sigma_s \cos \theta) \sin(\pi x_1) \sin(\pi x_2) \sin(\pi x_3) \\ & + 10\pi \omega_3^2 \sin(\pi x_1) \sin(\pi x_2) \cos(\pi x_3) + 10\pi \omega_2 \omega_3 \sin(\pi x_1) \cos(\pi x_2) \sin(\pi x_3) \\ & + 10\pi \omega_1 \omega_3 \cos(\pi x_1) \sin(\pi x_2) \sin(\pi x_3). \end{aligned}$$

We take $\sigma_t = 3$ and $\sigma_s = 1$ in the numerical calculations.

TABLE 5.4
Error $\|u - u_h\|_h$ *for Example 5.2.*

h	$c_p = 0$	$c_p = .01$	$c_p = .1$	$c_p = 1$	$c_p = 10$
$\frac{\sqrt{2}}{2}$	0.621343	0.619260	0.619305	0.821279	1.240676
$\frac{\sqrt{2}}{3}$	0.360653	0.359518	0.359870	0.450734	0.608365
$\frac{\sqrt{2}}{5}$	0.156827	0.155823	0.153460	0.178368	0.211289
$\frac{\sqrt{2}}{7}$	0.087243	0.085895	0.082512	0.092398	0.103939
$\frac{\sqrt{2}}{10}$	0.047717	0.045806	0.042170	0.045844	0.050153

TABLE 5.5
Error $\|\|u - u_h\|\|_h$ *for Example 5.2.*

h	$c_p = 0$	$c_p = .01$	$c_p = .1$	$c_p = 1$	$c_p = 10$
$\frac{\sqrt{2}}{2}$	2.034105	0.777330	1.110380	1.790423	1.759724
$\frac{\sqrt{2}}{3}$	1.340891	0.461619	0.682265	1.045150	0.894685
$\frac{\sqrt{2}}{5}$	0.720299	0.208898	0.333826	0.479858	0.329372
$\frac{\sqrt{2}}{7}$	0.459365	0.121339	0.203847	0.282646	0.173090
$\frac{\sqrt{2}}{10}$	0.281397	0.070559	0.121400	0.163126	0.091996

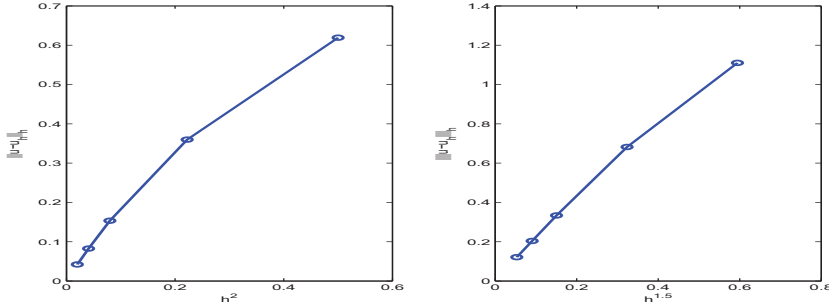


FIG. 5.3. *Example 5.2:* $\|u - u_h\|_h$ vs. h^2 (left) and $\|\|u - u_h\|\|_h$ vs. $h^{1.5}$ (right).

For $\eta = 0.1$, numerical results with the S_4 quadrature are reported in Tables 5.6, 5.7, and Figure 5.4. To see the influence of the numerical quadrature error on the solution accuracy, we also use the S_{12} quadrature for the numerical solution, and the numerical values are pretty close to those computed with the S_4 quadrature. For instance, corresponding to $c_p = 0.1$, the numerical solution errors $\|u - u_h\|_h$ for the five values of the meshsize h are, respectively, 0.725971, 0.347470, 0.133601, 0.069978, 0.034934; those for $\|\|u - u_h\|\|_h$ are, respectively, 1.191514, 0.644462, 0.298326, 0.179657, and 0.104885. Thus, the numerical solution errors in Tables 5.6 and 5.7 are mainly due to the spatial discretization.

For $\eta = 0.5$, numerical results with the S_4 quadrature are given in Tables 5.8 and 5.9. The numerical solution errors for smaller meshsize such as $h = \sqrt{2}/10$ are larger than expected, indicating that the S_4 quadrature is not accurate enough for this size of h . When the more accurate S_{12} quadrature is employed, there is a noticeable improvement in the solution accuracy for the meshsize $h = \sqrt{2}/10$. For instance, corresponding to $c_p = 0.1$, the numerical solution errors $\|u - u_h\|_h$ for the

TABLE 5.6
Error $\|u - u_h\|_h$ for Example 5.3 with $\eta = 0.1$.

h	$c_p = 0$	$c_p = .01$	$c_p = .1$	$c_p = 1$	$c_p = 10$
$\frac{\sqrt{2}}{2}$	0.742007	0.737949	0.723722	0.802436	0.964870
$\frac{\sqrt{2}}{3}$	0.357091	0.354543	0.346264	0.383675	0.442497
$\frac{\sqrt{2}}{5}$	0.137961	0.136739	0.132973	0.141812	0.151930
$\frac{\sqrt{2}}{7}$	0.072476	0.071751	0.069574	0.072776	0.076098
$\frac{\sqrt{2}}{10}$	0.036260	0.035854	0.034690	0.035799	0.036922

TABLE 5.7
Error $\|u - u_h\|_h$ for Example 5.3 with $\eta = 0.1$.

h	$c_p = 0$	$c_p = .01$	$c_p = .1$	$c_p = 1$	$c_p = 10$
$\frac{\sqrt{2}}{2}$	2.257263	0.922657	1.204273	1.603020	1.390244
$\frac{\sqrt{2}}{3}$	1.344653	0.453296	0.647719	0.862588	0.625379
$\frac{\sqrt{2}}{5}$	0.677586	0.184297	0.297870	0.382568	0.231471
$\frac{\sqrt{2}}{7}$	0.422869	0.102537	0.178835	0.225955	0.125866
$\frac{\sqrt{2}}{10}$	0.253594	0.055562	0.104207	0.130144	0.068043

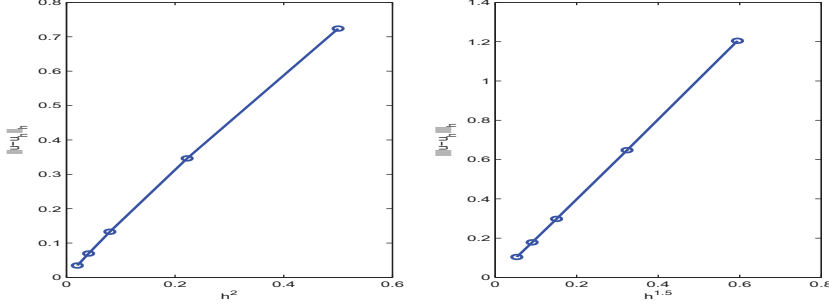


FIG. 5.4. Example 5.3 with $\eta = 0.1$: $\|u - u_h\|_h$ vs. h^2 (left) and $\|u - u_h\|_h$ vs. $h^{1.5}$ (right).

TABLE 5.8
Error $\|u - u_h\|_h$ for Example 5.3 with $\eta = 0.5$.

h	$c_p = 0$	$c_p = .01$	$c_p = .1$	$c_p = 1$	$c_p = 10$
$\frac{\sqrt{2}}{2}$	0.744114	0.739876	0.725580	0.808357	0.979578
$\frac{\sqrt{2}}{3}$	0.358188	0.355537	0.347206	0.386449	0.446200
$\frac{\sqrt{2}}{5}$	0.141961	0.140728	0.137036	0.146368	0.156864
$\frac{\sqrt{2}}{7}$	0.081168	0.080498	0.078554	0.081929	0.085397
$\frac{\sqrt{2}}{10}$	0.052538	0.052248	0.051461	0.052530	0.053599

five values of the meshsize h are, respectively, 0.731638, 0.349597, 0.134124, 0.070175, and 0.035002; those for $\|u - u_h\|_h$ are, respectively, 1.196005, 0.646826, 0.299145, 0.180041, and 0.105050. The corresponding plots are shown in Figure 5.5.

In the above numerical examples, the true solutions are smooth so that the regularity conditions (4.12) and (4.20) hold for any r and r' . Since linear elements are

TABLE 5.9
Error $\|u - u_h\|_h$ for Example 5.3 with $\eta = 0.5$.

h	$c_p = 0$	$c_p = .01$	$c_p = .1$	$c_p = 1$	$c_p = 10$
$\frac{\sqrt{2}}{2}$	2.275446	0.927688	1.211093	1.609242	1.401517
$\frac{\sqrt{2}}{3}$	1.355385	0.457630	0.652697	0.867074	0.628389
$\frac{\sqrt{2}}{5}$	0.683392	0.191211	0.303129	0.386956	0.237341
$\frac{\sqrt{2}}{7}$	0.428030	0.114502	0.186498	0.232227	0.136114
$\frac{\sqrt{2}}{10}$	0.259759	0.075458	0.116321	0.140127	0.085306

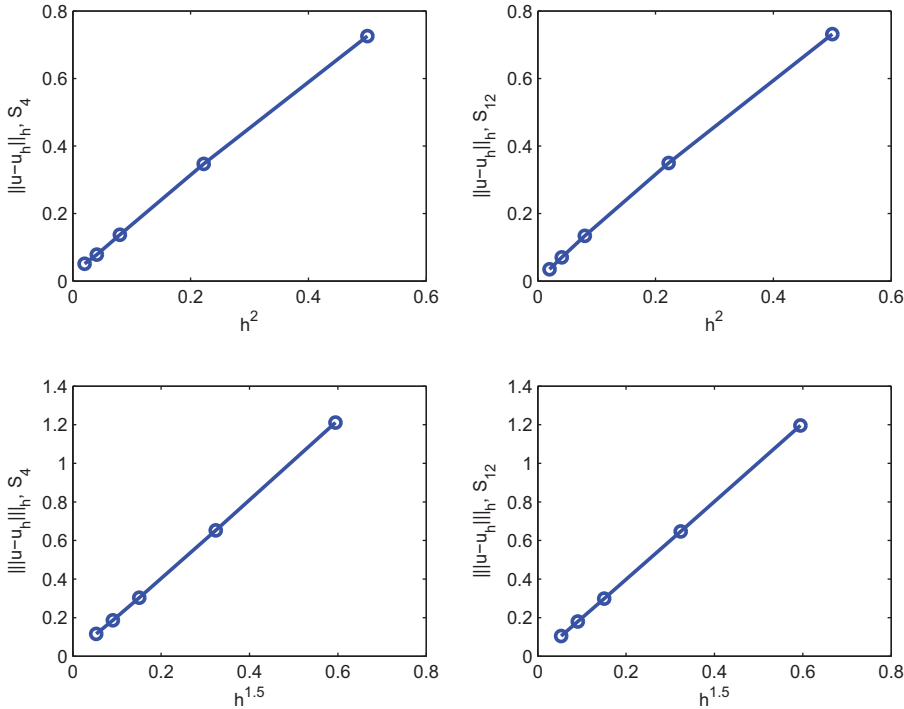


FIG. 5.5. *Example 5.3 with $\eta = 0.5$: $\|u - u_h\|_h$ vs. h^2 and $\|u - u_h\|_h$ vs. $h^{1.5}$, for S_4 quadrature and S_{12} quadrature.*

used, the theoretical results from Theorems 4.6 and 4.7 predict the convergence order for the numerical solution of the semidiscrete system (3.7), measured in the norm $\|\cdot\|_h$, is 1.5. We observe that in all the examples, numerically it is evident that $\|u - u_h\|_h = O(h^{1.5})$. Also, as long as the numerical integration on the sphere is done accurately enough, numerically it is evident that $\|u - u_h\|_h = O(h^2)$.

From the results of the above numerical examples, we observe that the inclusion of the stabilization terms in the bilinear form leads to improvement in solution accuracy if the penalty parameter c_p is chosen properly. In the examples, $c_p = 0.01$ and $c_p = 0.1$ are good choices. Larger values of c_p increase the numerical solution errors and slow down convergence of or even lead to divergence of iteration methods employed in solving the discretized systems.

6. Discussions and conclusions. The RTE appears in a wide variety of applications. It is a serious challenge to solve the RTE accurately due to the high dimension of the independent variables. In this paper, we develop discrete-ordinate DG methods for solving the RTE. The discrete ordinate technique is applied to discretize the integration over the unit sphere, and DG discretization is used for the spatial differentiation. For the numerical methods, with or without a stabilization term, we show rigorously the stability property and unique solvability of the discrete systems. Under suitable solution regularity assumptions, we derive error estimates for the numerical solutions. Results from several numerical examples illustrate the good convergence behavior of the methods. When the penalty parameter is chosen properly, the method with the stabilization term provides more accurate numerical results.

While the investigations of some basic aspects of the discrete-ordinate DG methods in this paper indicate the methods are promising in solving the RTE, much remains to be done in the future, e.g., the optimal or near-optimal choice of the penalty parameter in the formulation, a posteriori error estimation and adaptive algorithms for simultaneous spatial mesh refinement and proper selection of numerical quadratures on the unit sphere, effective parallel implementation of the algorithms, and applications in solving RTE-based inverse problems that arise in physical and biological sciences.

Acknowledgments. The authors thank the two anonymous referees for their valuable comments and suggestions. The second author's work was conducted while he was a visiting professor at Department of Mathematics, University of Iowa; the second author expresses his gratitude for the hospitality of the department.

REFERENCES

- [1] R. A. ADAMS, *Sobolev Spaces*, Academic Press, New York, 1975.
- [2] A. AGOSHKOV, *Boundary Value Problems for Transport Equations*, Birkhäuser, Boston, 1998.
- [3] D. N. ARNOLD, F. BREZZI, B. COCKBURN, AND L. D. MARINI, *Unified analysis of discontinuous Galerkin methods for elliptic problems*, SIAM J. Numer. Anal., 39 (2002), pp. 1749–1779.
- [4] M. ASADZADEH AND A. KADEM, *Chebyshev spectral— S_N method for the neutron transport equation*, Comput. Math. Appl., 52 (2006), pp. 509–524.
- [5] K. ATKINSON, *Numerical integration on the sphere*, J. Aust. Math. Soc. Ser. B, 23 (1982), pp. 332–347.
- [6] K. ATKINSON AND W. HAN, *Theoretical Numerical Analysis: A Functional Analysis Framework*, 3rd ed., Springer, New York, 2009.
- [7] G. BAL AND A. TAMASAN, *Inverse source problems in transport equations*, SIAM J. Math. Anal., 39 (2007), pp. 57–76.
- [8] S. C. BRENNER AND L. R. SCOTT, *The Mathematical Theory of Finite Element Methods*, 3rd ed., Springer, New York, 2008.
- [9] F. BREZZI, B. COCKBURN, L.D. MARINI, AND E. SÜLI, *Stabilization mechanisms in discontinuous Galerkin finite element methods*, Comput. Methods Appl. Mech. Engrg., 195 (2006), pp. 3293–3310.
- [10] F. BREZZI, L. D. MARINI, AND E. SÜLI, *Discontinuous Galerkin methods for first-order hyperbolic problems*, Math. Models Methods Appl. Sci., 14 (2004), pp. 1893–1903.
- [11] B. G. CARLSON AND K. D. LATHROP, *Transport theory—the method of discrete ordinates*, in Computing Methods in Reactor Physics, H. Greenspan, C. N. Kelber, and D. Okrent, eds., Gordon and Breach, New York, 1968, pp. 171–266.
- [12] B. CHANG, T. MANTEUFFEL, S. MCCORMICK, J. RUGE, AND B. SHEEHAN, *Spatial multigrid for isotropic neutron transport*, SIAM J. Sci. Comput., 29 (2007), pp. 1900–1917.
- [13] P. G. CIARLET, *The Finite Element Method for Elliptic Problems*, North-Holland, Amsterdam, 1978.
- [14] B. COCKBURN, *Discontinuous Galerkin methods*, ZAMP Z. Angew. Math. Mech., 83 (2003), pp. 731–754.

- [15] B. COCKBURN, *Discontinuous Galerkin methods for computational fluid dynamics*, in Encyclopedia of Computational Mechanics, Vol. 3, E. Stein, R. de Borst, and T. J. R. Hughes, eds., John Wiley & Sons, New York, 2004, pp. 91–127.
- [16] B. COCKBURN, G. E. KARNIADAKIS, AND C.-W. SHU (EDS.), *Discontinuous Galerkin methods. Theory, Computation and Applications*, Lect. Notes Comput. Sci. Eng. 11, Springer, New York, 2000.
- [17] P. EDSTRÖM, *A fast and stable solution method for the radiative transfer problem*, SIAM Rev., 47 (2005), pp. 447–468.
- [18] W. FREEDEN, T. GERVEN, AND M. SCHREINER, *Constructive Approximation on the Sphere with Applications to Geomathematics*, Oxford University Press, Oxford, 1998.
- [19] W. HAN, J. A. EICHHOLZ, J. HUANG, AND J. LU, *RTE based bioluminescence tomography: A theoretical study*, submitted.
- [20] L. HENYNEY AND J. GREENSTEIN, *Diffuse radiation in the galaxy*, Astrophys. J., 93 (1941), pp. 70–83.
- [21] K. HESSE AND I. H. SLOAN, *Cubature over the sphere S^2 in Sobolev spaces of arbitrary order*, J. Approx. Theory, 141 (2006), pp. 118–133.
- [22] C. JOHNSON AND J. PITKÄRANTA, *An analysis of the discontinuous Galerkin method for a scalar hyperbolic equation*, Math. Comp., 46 (1986), pp. 1–26.
- [23] A. D. KIM AND M. MOSCOSO, *Chebyshev spectral methods for radiative transfer*, SIAM J. Sci. Comput., 23 (2002), pp. 2074–2094.
- [24] P. LESAINT AND P. A. RAVIART, *On a finite element method for solving the neutron transport equation*, in Mathematical Aspects of Finite Elements in Partial Differential Equations, C. A. de Boor, ed., Academic Press, New York, 1974, pp. 89–123.
- [25] E. E. LEWIS AND W. F. MILLER, *Computational Methods of Neutron Transport*, John Wiley & Sons, New York, 1984.
- [26] E. MACHORRO, *Discontinuous Galerkin finite element method applied to the 1-D spherical neutron transport equation*, J. Comput. Phys., 223 (2007), pp. 67–81.
- [27] M. F. MODEST, *Radiative Heat Transfer*, 2nd ed., Academic Press, New York, 2003.
- [28] F. NATTERER AND F. WÜBBELING, *Mathematical Methods in Image Reconstruction*, SIAM, Philadelphia, 2001.
- [29] W. H. REED AND T. R. HILL, *Triangular Mesh Methods for the Neutron Transport Equation*, Technical report LA-UR-73-479, Los Alamos National Laboratory, Los Alamos, NM, 1973.
- [30] A. H. STROUD, *Approximate Calculation of Multiple Integrals*, Prentice-Hall, Englewood Cliffs, NJ, 1971.
- [31] G. E. THOMAS AND K. STAMNES, *Radiative Transfer in the Atmosphere and Ocean*, Cambridge University Press, London, 1999.
- [32] W. ZDUNKOWSKI, T. TRAUTMANN, AND A. BOTT, *Radiation in the Atmosphere: A Course in Theoretical Meteorology*, Cambridge University Press, London, 2007.